Evaluation of the Uncertainty in JP-7 Kinetics Models Applied to Scramjets

A. T. Norris, †
NASA Langley Research Center, Hampton, Virginia, 23681

ABSTRACT

One of the challenges of designing and flying a scramjet-powered vehicle is the difficulty of preflight testing. Ground tests at realistic flight conditions introduce several sources of uncertainty to the flow that must be addressed. For example, the scales of the available facilities limit the size of vehicles that can be tested and so performance metrics for larger flight vehicles must be extrapolated from ground tests at smaller scales. To create the correct flow enthalpy for higher Mach number flows, most tunnels use a heater that introduces vitiates into the flow. At these conditions, the effects of the vitiates on the combustion process is of particular interest to the engine designer, where the ground test results must be extrapolated to flight conditions.

In this paper, the uncertainty of the cracked JP-7 chemical kinetics used in the modeling of a hydrocarbon-fueled scramjet was investigated. The factors that were identified as contributing to uncertainty in the combustion process were the level of flow vitiation, the uncertainty of the kinetic model coefficients and the variation of flow properties between ground testing and flight. The method employed was to run simulations of small, unit problems and identify which variables were the principal sources of uncertainty for the mixture temperature. Then using this resulting subset of all the variables, the effects of the uncertainty caused by the chemical kinetics on a representative scramjet flow-path for both vitiated (ground) and nonvitiated (flight) flows were investigated.

The simulations showed that only a few of the kinetic rate equations contribute to the uncertainty in the unit problem results, and when applied to the representative scramjet flowpath, the resulting temperature variability was on the order of 100 K. Both the vitiated and clean air results showed very similar levels of uncertainty, and the difference between the mean properties were generally within the range of uncertainty predicted.

INTRODUCTION

Scramjet-powered vehicles pose a unique challenge to designers in many ways. One of the major challenges is that the ability to refine a design and improve operability via ground testing is a very difficult process. Ground test facilities for anything but the smallest vehicles are too small to test the whole flight assembly and the test conditions are often only an approximation of what the flight conditions are. For example, ground facilities often have vitiates created in the airflow in order to obtain realistic flight enthalpies. The vitiates are created when the inflow air is heated via combustion, the oxygen used burning the fuel is replaced, and the resulting inflow contains a certain amount of combustion products. To bridge the gap between the ground tests and flight performance, modeling is being relied on to an increasing level. With this usage comes the question of how much uncertainty is in the models used to simulate the flight vehicles? This question has resulted in a significant effort in the past few years to try and quantify the uncertainty found in modeling flight vehicles, and specifically the ability to extrapolate ground test data to predict flight performance. One product of this has been the JANNAF Uncertainty Quantification Report[1] that looked at the methods and processes of estimating the uncertainty of models. Another manifestation of the importance being attached to this issue is the formation of the Uncertainty Quantification Technical Challenge group under the NASA Hypersonic Technology Project.

† Aerospace Engineer, Hypersonic Airbreathing Propulsion Branch, NASA Langley

While it is somewhat daunting to try and consider all the factors that can contribute to the uncertainty in modeling scramjet powered vehicles, it is a useful starting point to consider discrete parts of the problem. To that end, this paper will look at the uncertainty between ground and flight of the combustion process for a hydrocarbon fueled scramjet. This will involve evaluating the uncertainty in the chemical kinetics and flow properties and also looking at the effect vitiation has on this process.

UNCERTAINTY IN COMBUSTION MODELING

The combustion process in scramjet engines is a complex system to understand and model. The fuel and air have to mix rapidly to ensure the combustion occurs before the reacting mixture exits the engine, and stable flame holding regions have to be established to ensure robust operation of the engine, all the while ensuring the combustion and resulting pressure rise does not unstart the engine. In addition to providing the energy to generate propulsion, the fuel can also be called upon to cool the engine structure. For liquid hydrogen fuel, this cooling process is relatively simple from a thermodynamic and chemical point of view. However, current research is focused on hydrocarbon-fueled scramjets that results in further modeling challenges due to the more complex molecular form of the fuel.

One of the effects of using complex hydrocarbons for cooling is that pyrolysis (or cracking) of the fuel occurs as well as coking. JP-7 fuel was developed to minimize coking of the fuel lines and has been the hydrocarbon fuel of choice for current scramjets. However due to cracking, the fuel will enter the engine with a different molecular structure than when it was put in the fuel tank. It should be noted that JP-7 is a blend of many different hydrocarbon molecules and there is a variation in the exact chemical composition from batch to batch.

For investigating the performance of scramjet combustor components, such as flame holding cavities or injector concepts, the need to heat and crack JP-7 can add considerable complexity to a test facility. Thus, a surrogate cracked fuel has been developed that mimics the properties of the broken down JP-7. This surrogate mixture was developed by Pellet et al.[2] for the purpose of testing such scramjet components and consists of 36% methane and 64% ethylene by volume. This mixture was developed by matching the laminar opposed-jet flame properties of the surrogate mixture to those of the cracked JP-7.

In order to study the uncertainty inherent in modeling the combustion process in a hydrocarbon fueled scramjet, a suitable engine test case needs to be used where the geometry is simple (for computational reasons) and the fuel composition is well known. In this paper, the HIFiRE Direct Connect Rig (HDCR)[3,4] tested at NASA Langley was used. This test article was a ground-test version of a simple engine used in the HIFiRE Program[5] to demonstrate the operability of the flight design. The test article was operated in a direct-connect mode, and constructed of uncooled two-inch thick copper to ensure survivability for multiple ground tests. The rig was fueled with the surrogate cracked JP-7 mixture of Pellet et al. and a diagram of the flowpath is shown in Fig. (1).

For the kinetics of the cracked JP-7 surrogate, the 32 species, 206 reaction ethylene mechanism of Luo et al.[6] was used. The 206 reactions that make up this kinetic mechanism are generally represented by the Arrhenius form of the rate equation

$$k_f = AT^b exp{-E/RT}. \tag{1}$$

where A, b and E are experimentally obtained constants and listed in Appendix A, R is the universal gas constant and T is the mixture temperature. The uncertainty in the equation is most often represented by an uncertainty factor UF, which represents the maximum and minimum value for which k_f is bounded

$$k_f/UF < k_f < k_f * UF. \tag{2}$$

It should be noted that UF does not represent any statistical quantity or confidence limits, but rather is just a statement about what bounds the experimental data lies within. For the purposes of this study, UF is interpreted as a confidence limit of 95% (2σ). That is, it is expected that there is a 5% chance that k_f may

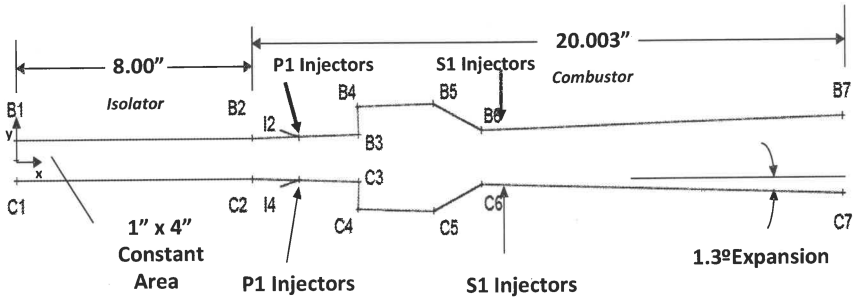

	x [mm (in.)]	y [mm (in.)]
C1	0.000	-12.7 (-0.500)
C2	203 (8.000)	-12.7 (-0.500)
C3	295 (11.596)	-14.8 (-0.582)
C4	294 (11.581)	-31.9 (-1.256)
C5	359 (14.150)	-33.4 (-1.315)
C6	401 (15.794)	17.2 (-0.677)
C7	711 (28.003)	-24.2 (-0.954)
B1	0.000	12.7 (0.500)
B2	203 (8.000)	12.7 (0.500)
B3	295 (11.596)	14.8 (0.582)
B4	294 (11.581)	31.9 (1.256)
B5	359 (14.150)	33.4 (1.315)
B6	401 (15.794)	17.2 (0.677)
B7	711 (28.003)	24.2 (0.954)
I2	244 (9.596)	13.6 (0.536)
I4	244 (9.596)	-13.6 (-0.536)

Figure 1. Sketch of the flowpath of the HDCR scramjet rig.

lay outside the limits. In addition, the form of UF lends itself to the assumption that k_f is distributed with a log-normal probability density function (PDF). For each of the 206 equations, the uncertainty factor was obtained from the literature.[7–9] For the case where no number could be found, a conservative value of 5 was chosen. The kinetic mechanism and the corresponding uncertainty factors are all listed in Appendix A.

In addition to reaction kinetics, two other variables are also considered for the uncertainty evaluation: pressure (P) and temperature (T). Using data from the NASA Langley Arc-Heated Scramjet Test Facility (AHSTF) where the HDCR was tested, these quantities were assumed to have a normal distribution, based on the symmetry of the data, with a standard deviation of 0.15 psi and 10 K, respectively. Mean values were chosen as corresponding to the conditions of the flow in the HDCR just before the onset of combustion. As well as being tested in the AHSTF, the HDCR was also tested in Test Bay IV of the ATK GASL Ronkonkoma blow-down test facility where the effects of vitiation were investigated.[10] In the GASL tests, the effect of different levels of vitiation, and also vitiate composition, on the performance of the HDCR were investigated. The composition of the methane-heated vitiated air was not reported for the GASL tests, and so the vitiation composition was taken from that used in the NASA Langley HTT, when operated at Mach 3.[11] The compositions of clean and vitiated air caused by combustion heating are listed in Table 1.

Table 1. Composition of vitiated vs. nonvitiated air used in simulations.

Species	Clean Air (Mass Fraction)	Vitiated Air (Mass Fraction)
CO2	0.0	0.0552
H2O	0.0	0.0455
O2	0.2330	0.2330
N2	0.7660	0.6663

UNCERTAINTY EVALUATION

The simplest approach to evaluating the uncertainty caused by chemical kinetics on the performance of the HDCR would be to perform multiple simulations, each time with the rate constants chosen randomly from their respective distributions. For the reaction variables (a log-normal distribution), the random rate constants are obtained by adjusting the A constant of the Arrhenius equation in the following manner:

$$\acute{A}_i = exp(\mathcal{R} * UF/2 + \ln(A_i)), \tag{3}$$

where $\acute{A}_i$ is the new adjusted rate constant of the ith reaction, $\mathcal{R}$ is a random number with a normal distribution and the value 2 reflects the 2σ confidence limit. A similar method is employed for the two properties, P and T, except with a normal distribution rather than a log-normal PDF. Due to the large number of variables, this method requires an enormous number of simulations and would take a very long time to complete. Instead, a couple of simple test cases were used to evaluate the sensitivity of the rate equations and provide an indication of which variables really mattered in the combustion process. Then a small set of representative rate equations were used to perform simulations on the HDCR geometry.

The first simple test case considered was the evaluation of the ignition delay time. In this test, a mixture of fuel and air is placed in a reactor at constant pressure and allowed to react. After a certain period of time there is a sudden rise in temperature as the fuel ignites; this time is referred to as the ignition delay time (τ_i). A series of typical ignition delay curves are shown in Fig. (2).

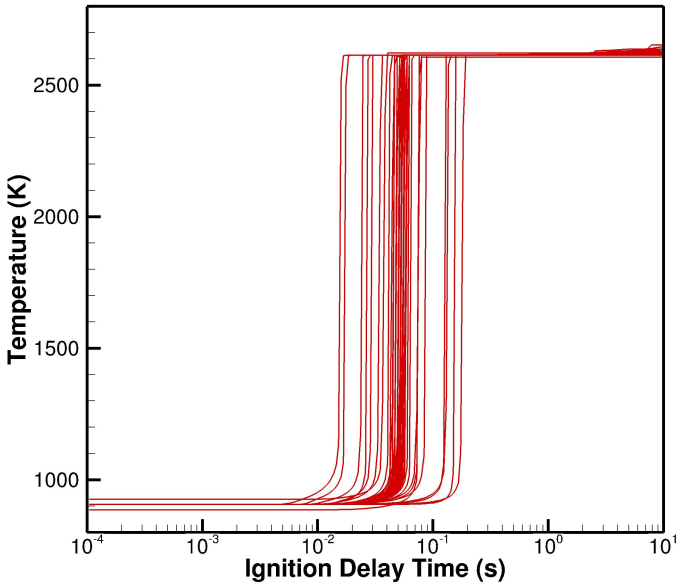

Figure 2. Typical ignition delay curves for a variety of reaction rates.

Three sets of fuel-air mixtures were chosen for this study for both vitiated and clean air flows: a lean mixture, a stoichiometric mixture and a rich mixture. The lean and rich mixture fractions were chosen as roughly the midpoint in composition between stoichiometric and the flammability limits. The initial conditions for the mixture were chosen as corresponding to the pressure and temperature of the flow just upstream of the reacting region of the HDCR. Using the three fuel-air mixtures and a series of randomly selected rate and property variables obtained from the PDFs defined above, the rate equations were integrated until the mixture ignited. In this case, ignition was defined as when the mixture temperature reached 1500K, which is the midpoint between the unburnt and burnt mixture temperatures. Details of the compositions and the results of the tests are shown in Table 2. Of interest is that the trend of the vitiated mixtures to have a slightly smaller ignition delay, which is opposite of that found by Sklar.[10] However, the difference is well within the uncertainty margin of the results and the kinetic model used by Sklar is not reported.

For a Monte Carlo simulation like this, a convergence test is needed to see if enough simulations have been performed. In this case, the criterion used was to perform simulations until the variance of the mean ignition time had reached a statistically steady state. The results of this test are shown in Fig. (3) where it can be seen that the variance of the mean ignition time has become steady by about 5,000 simulations.

Table 2. Uncertainty of the Monte Carlo ignition delay simulations for the different flow conditions.

Ignition Test	Mean Ignition Delay (s)	Std. Deviation
Nonvitiated		
Lean ϕ = 0.65	4.75e-02	2.70
Stoichiometric ϕ = 1.0	5.15e-02	2.95
Rich ϕ = 2.45	2.05e-01	2.85
Vitiated		
Lean ϕ = 0.65	4.40e-02	2.65
Stoichiometric ϕ = 1.0	4.70e-02	2.95
Rich ϕ = 2.45	1.70e-01	2.90

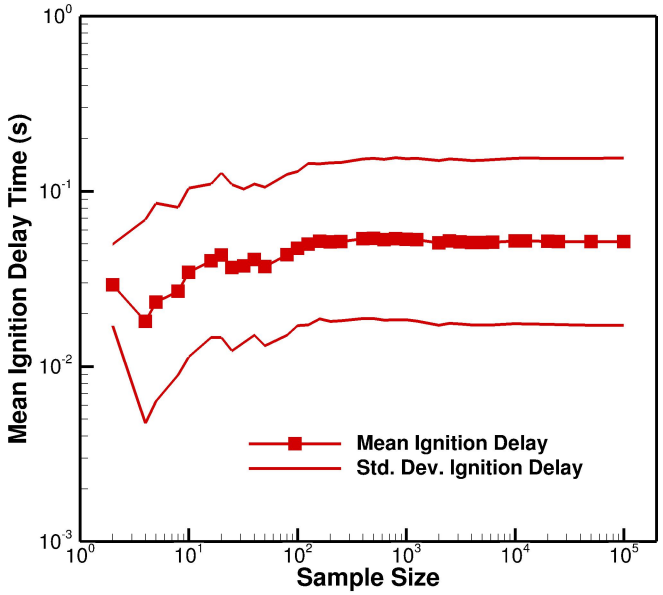

Figure 3. Convergence of the Monte Carlo simulation as a function of sample size.

Having established that a statistically steady state has been reached, the relative effect of each rate equation on the ignition delay time needs to be evaluated. To perform this, the correlation r_j between the value of the jth randomly selected variable and the resulting ignition delay time is calculated for all the i trials

$$r_j = \frac{1}{\sigma_A \sigma_\tau} \sum_{i=1}^{N} (\acute{A_{j,i}} - \overline{A_j})(\tau_i - \overline{\tau}), \tag{4}$$

where σ_A and σ_τ are the standard deviation of $\acute{A_j}$ and τ, respectively, $\overline{\acute{A_j}}$ is the mean value of $\acute{A_j}$ and $\overline{\tau}$ is the mean ignition delay time. Note also that j is the index of the rate equation, and i is summed over the N trials. In addition, the temperature and pressure correlations are also obtained by a similar manner. These correlations are plotted in Fig. (4) for the stoichiometric, clean air case. Note that the last two entries plotted are the temperature and pressure. The results for the lean and rich cases were also calculated for both vitiated and nonvitiated air.

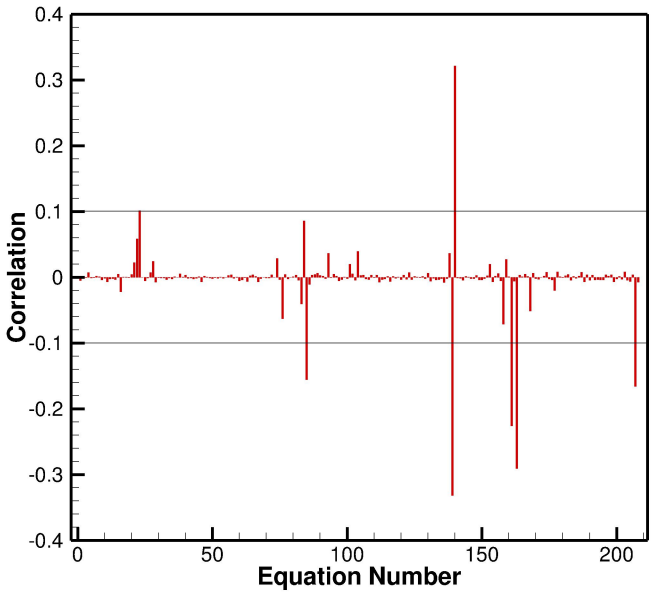

Figure 4. Bar Graph showing correlation of reaction rate equations to ignition delay time for stoichiometric, nonvitiated mixture for all 206 rate equations and the temperature and pressure (last two bars).

It can be seen in Fig. (4) that the correlation for all but a few variables is very small, and so can be ignored. Taking a cut-off limit of $\mid 0.1 \mid$, the 208 random variables can be reduced to the seven variables that have the largest effect on the ignition delay time (6 reaction variables and the temperature). The results of the lean and rich correlations were very similar to the stoichiometric results, with rate equation 158 being the only additional significantly correlated reaction rate variable, and so this rate variable was included. Using these resulting seven rate equation variables and the temperature, two new reaction mechanisms can be put forward where the constants have been adjusted to create a slow and a fast mechanism. The equation numbers that have been adjusted and new values for the A constant are shown in Table 3. The results of using these new slow and fast reaction mechanisms for an ignition delay test is shown in Fig. (5). Compared to the values of uncertainty obtained from the Monte Carlo simulations shown in Table 2, the two mechanisms bound the baseline value at about the 95% confidence level.

The second test case was the Perfectly Stirred Reactor (PSR). A PSR is a simple, zero-dimensional model that is very useful for the investigation of chemical reactions. It consists of a volume, V, at pressure, P, containing a mass m^r. Into this volume, fuel and oxidizer are supplied at a fixed rate, $\dot{m}^{in}$. Inside, the fuel and oxidizer mix instantly with the contents of the reactor and react. Finally, there is a fixed rate of mass leaving the reactor, $\dot{m}^{out}$.

For a given volume and mass flow in and out of the reactor, the residence time scale for the reactor can be calculated:

$$\tau_r = \frac{m^r}{\dot{m}^{in}} = \frac{m^r}{\dot{m}^{out}}. \tag{5}$$

This time scale can be thought of as the amount of time the species stay in the reactor before leaving, or alternately as the ratio of the mass of fluid in the reactor to the mass of fluid entering or exiting the reactor.

The behavior of a PSR is consistent for most chemical reactions of interest to the combustion community. The mass contained in the reactor volume is given by ρV, where ρ is the density of the fluid. For the case of

Table 3. Most correlated rate equations and adjusted A constants for slow and fast reaction mechanisms obtained from the ignition delay test.

Equation	UF	A_{slow}	A_{fast}
23	3.0	1.26e+15	1.4e+14
85	5.0	2.68e+12	6.7e+13
139	5.0	6.0e+10	1.5e+12
140	3.16	1.45e+17	1.45e+16
158	5.0	3.02e+06	7.55e+07
161	4.0	9.0e+05	1.44e+07
163	5.0	4.0e+11	1.0e+13
Temperature Uncertainty			
207	20K	883K	923K

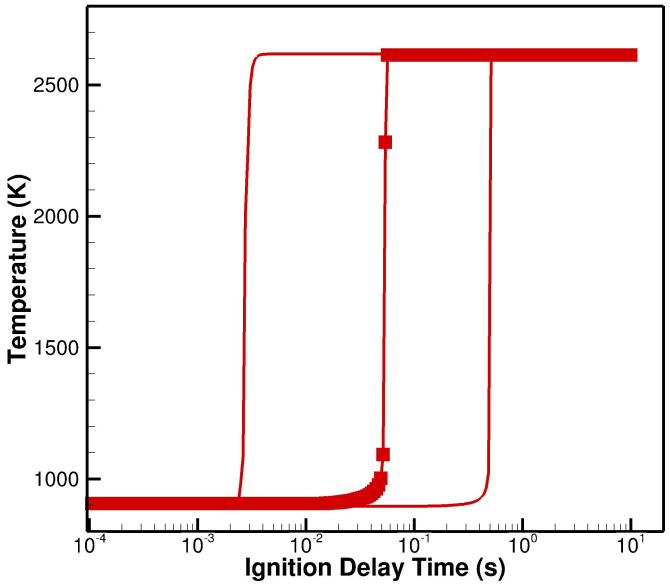

Figure 5. Ignition delay plot for slow and fast reaction mechanisms compared to baseline (symbols) case.

a large residence time, ρV is large compared to $\dot{m}^{in}$ and so the fluid in the reactor has a long time to react before it leaves. In this case, the reactor has a composition close to fully reacted. For the case where τ_r is small, the fluid has very little time to react before it exits the reactor, and so the composition in the reactor is essentially unreacted.

The plot of temperature vs. residence time for several typical PSR simulations is shown in Fig. (6). It can be seen that for large residence times, the temperature of the reactor is that of a fully reacted, or equilibrium mixture. As the residence time becomes smaller, the temperature drops slightly before a sudden drop-off to fully unreacted, which is typical of most hydrocarbon-air reactions. The residence time when the mixture ceases to react is referred to as the blow-out limit, τ_b.

In a very similar way to that described for the ignition delay test, a Monte Carlo simulation was performed

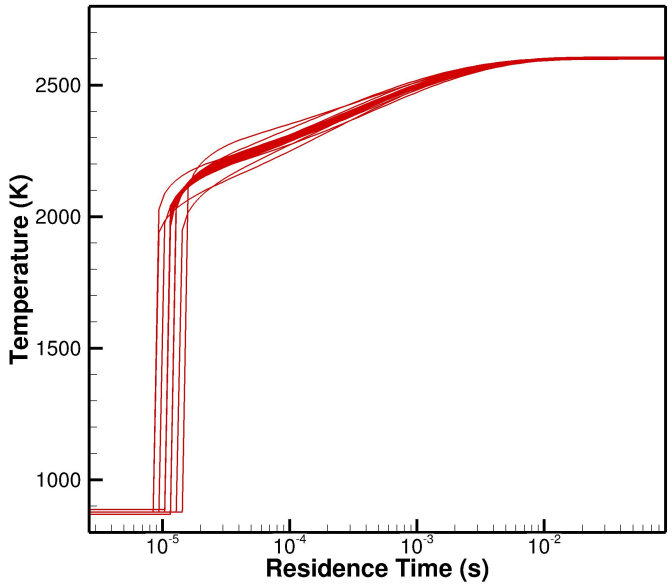

Figure 6. The temperature of the mixture in a perfectly-stirred reactor as a function of the residence time of the mixture for a variety of reaction rates.

using the 206 rate equations, temperature and pressure for a variety of flow conditions to establish the uncertainty of the predicted blow-out time. Blow-out was defined as the time when the temperature dropped below 1,500K. A convergence test was also performed and showed similar results to that of the ignition delay test. Results of the Monte Carlo tests are shown in Table 4. The results here show that vitiation makes the blow-out time smaller for a stoichiometric mixture, but there is a slight increase for both lean and rich mixtures.

Table 4. Uncertainty of the Monte Carlo PSR simulations for different flow conditions..

PSR Test	Mean Blow-out Time (s)	Std. Deviation
Nonvitiated		
Lean ϕ = 0.65	1.93e-05	1.36
Stoichiometric ϕ = 1.0	1.70e-05	1.23
Rich ϕ = 2.45	2.63e-05	1.23
Vitiated		
Lean ϕ = 0.6	2.02e-05	1.35
Stoichiometric ϕ = 1.0	1.28e-05	1.22
Rich ϕ = 2.45	3.00e-05	1.23

Correlations between the individual reaction rates and the blow-off time were also performed, and the results for the clean-air stoichiometric case are shown in Fig. (7). Unlike the ignition delay test, there were some differences in the significantly-correlated reaction rates between the lean, stoichiometric and rich flow conditions. Because of this, the selection criteria was changed to the correlations that are above the $\mid 0.1 \mid$ cut-off level and appear in at least two of the three flow conditions. The reactions selected and the resulting slow and fast mechanisms are shown in Table 5.

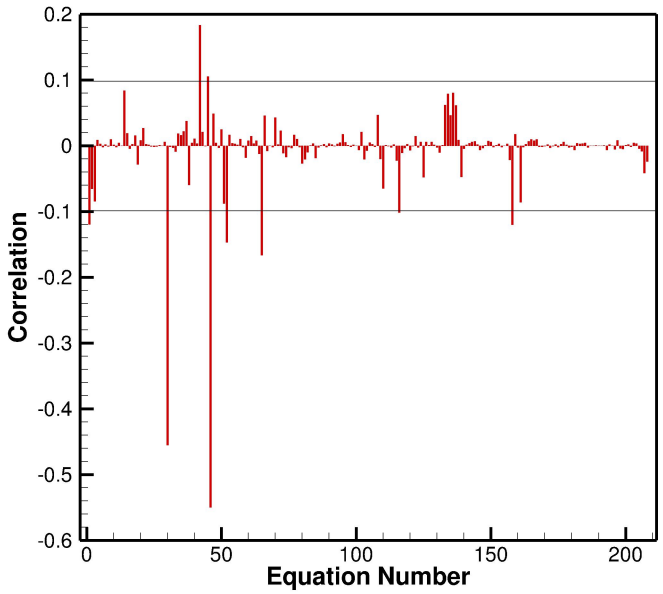

Figure 7. Bar Graph showing correlation of reaction rate equations to ignition delay time for stoichiometric, vitiated mixture.

Table 5. Most correlated rate equations and adjusted A constants for slow and fast reaction mechanisms obtained from the PSR test.

Equation	Uf	A_{slow}	A_{fast}
14	3.16	5.22e+18	5.22e+19
30	3.16	1.5e+08	1.5e+07
42	2.0	3.67e+13	1.468e+14
46	3.16	5.9e+17	5.9e+16
52	5.0	1.32e+13	5.28e+11
65	5.0	1.4e+14	5.6e+12

Using the slow and fast reaction mechanisms, the PSR simulation was performed and the results are shown in Fig. (8) compared to the baseline mechanism. Like the ignition delay test, the results show that the fast and slow mechanisms approximately bound the 95% confidence limit for the reactor simulation.

HDCR SIMULATION

For the purposes of this study, a subset of the engine flowpath was used. This was a one-inch wide slice taken on the side of the centerline that encompasses one primary and one secondary injector. The computational domain also invoked the symmetry of the flowpath, thus only gridding one eighth of the total flowpath. The reason for restricting the flow domain to a subset of the whole was to ensure that calculations involving large numbers of species and reactions could be finished in a reasonable time. The grid contains about 250,000 cells and extends from the facility plenum, through the nozzle and engine, finishing at the test article exit plane. The computational domain is shown in Fig. (9) and boundary conditions are listed below

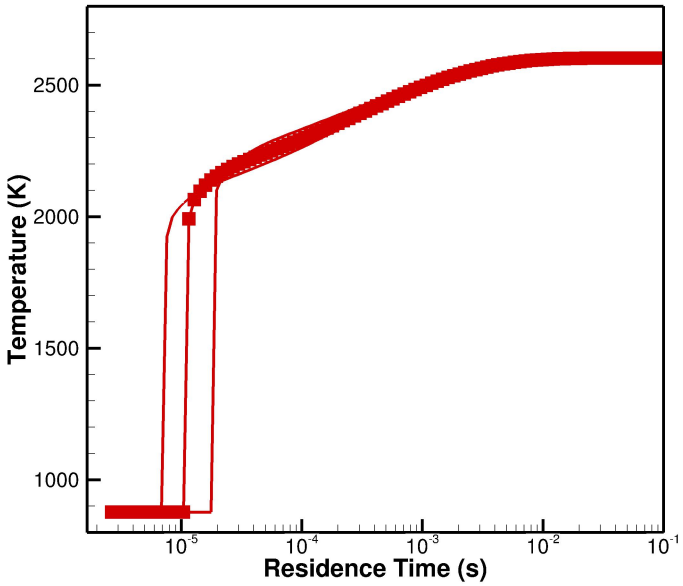

Figure 8. PSR temperature plot for the slow and fast reaction mechanisms compared to the baseline case (symbols).

in Table 6. Note that for both the vitiated and clean air flows, the mass flow rates are identical, however this means the Mach numbers differ slightly.

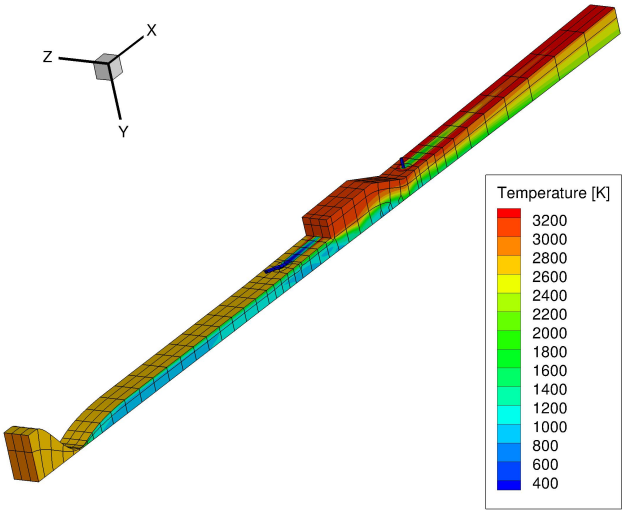

Figure 9. Plot of the computational domain used for the HDCR simulations.

Table 6. HDCR Boundary and inlet conditions

BC	Value
Inflow	Density = 5.27535 kg/m^3
	Velocity = 50 m/s
	Pressure = 4276817 Pa
Primary Injector	Density = 7.49750 kg/m^3
	Velocity = 50.0 m/s
	Temperature = 290.64 K
Secondary Injector	Density = 2.9124 kg/m^3
	Velocity = 7.790 m/s
	Temperature = 343.28 K
Wall	Adiabatic

The solution was performed using VULCAN-CFD[12] to solve the steady RANS equations. Wall functions were used for the no-slip walls, and the Menter Baseline turbulence model was used. Due to the need to solve a very large chemical kinetics model, no grid resolution studies were performed. However, as the goal was to just compare solutions of different kinetic models to each other, this was not considered an issue. The test conditions chosen were those for a simulated Mach 8 flight velocity, corresponding to an isolator entrance Mach number of 3.5. Simulations were performed for both vitiated and nonvitiated flows using the five different reaction kinetic schemes developed above. This meant a total of 10 different simulations were performed.

In comparing the results, the quantities of interest were the pressure profiles at the wall, the thrust, and the 1D integrated flow quantities. Due to the simplification of the flowpath for computational reasons and the different vitiate composition to that reported by the GASL experiments,[10] no quantitative comparison to experimental data can be made. However, certain trends in performance can be compared.

The first quantities examined are the wall pressure profiles, taken at the centerline of the chosen domain. These are shown in Fig. (10). As expected, there is no difference between the two flows upstream of the cavity, except for the effects of vitiation. In the region where the combustion occurs, differences caused by the different chemistry mechanisms are observed. Overall, a fairly consistent margin of uncertainty exists around the baseline reaction for both the vitiated and nonvitiated simulations, equal to about 10% of the pressure value. Also of interest is that the vitiated mechanisms, for the most part, show a pressure range just outside that bounded by the uncertainty of the nonvitiated mechanism. From this, it can be concluded that the effects of vitiation on pressure are comparable to the uncertainty of the chemical mechanism. It can also be noted that the use of reduced mechanisms can be justified if the results should fit within the uncertainty values of the full mechanism.

The results of the thrust for the different mechanisms are listed below in Table 7. Overall, the effect of the vitiation on the net thrust was to lower it by about 20%, which is the same effect seen in a study of hydrogen-fueled scramjets[13] and also the same trend seen in the GASL tests.[10] It is of interest that the viscous drag forces were increased by the vitiation, though their sensitivity to the uncertainty in the chemical kinetics was negligible. However, the axial pressure force did show variation with the different kinetic models, with the same trends for both vitiated and nonvitiated flows. While it is not possible to separate the effects of the kinetics and the changed thermal properties of the fluid due to vitiation, a tentative conclusion from this result is that, absent a large change in flow conditions, the uncertainty in the chemical kinetics does not have an effect on the viscous force, but only on the pressure force.

The final quantities of interest are the one-dimensional, mass-averaged quantities. The results for temperature, Mach number and pressure are shown in Fig. (11). The temperature results show that there is an uncertainty in the maximum temperature of about 200 K for both the clean air and vitiated cases observed over the whole range of temperatures, that gives a reacting uncertainty of about 10%. It is interesting that

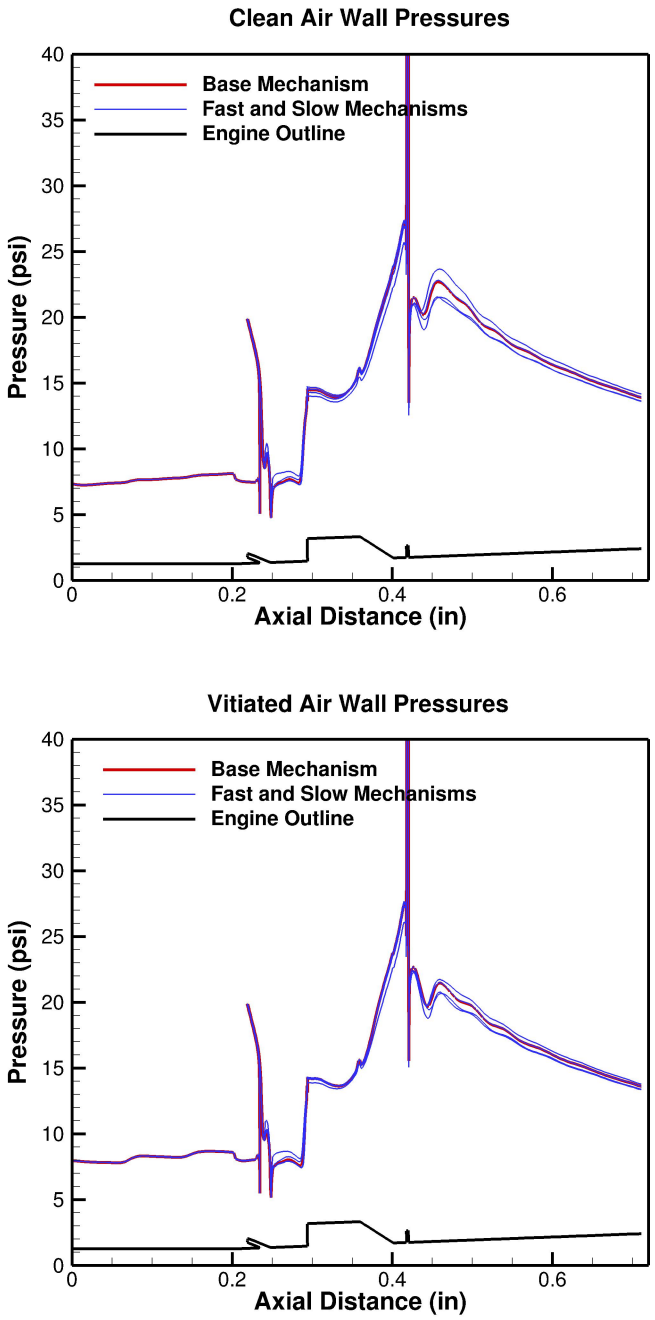

Figure 10. Centerline wall pressure plots for the different reaction mechanisms and for the vitiated and nonvitiated cases. Note location of injectors.

there is not much difference between the vitiated and nonvitiated profiles except for the trend of the vitiated to be a little lower for the quantities plotted in Fig. (11).

A similar conclusion can be obtained from the 1D Mach number, with the level of uncertainty only on the order of about 3%, while vitiation effects were not that significant. The 1D pressure results are very

Table 7. Net thrust for each reaction mechanism and flow condition. Note. Negative thrust is drag.

Simulation	Pressure Force (N)	Viscous Force (N)	Net Force (N)
	Non-Vitiated		
Base	17.249	-10.014	7.2351
Slow ID	17.230	-10.02	7.2091
Slow PSR	16.890	-10.000	6.8866
Fast ID	18.060	-9.852	8.2159
Fast PSR	17.933	-10.001	7.9310
	Vitiated		
Base	16.452	-10.400	6.0502
Slow ID	16.450	-10.410	6.0381
Slow PSR	16.060	-10.410	5.6520
Fast ID	17.180	-10.260	6.9130
Fast PSR	16.930	-10.390	6.5390

similar to the wall pressure profiles with the vitiation effects being more pronounced for this quantity and the uncertainty being around 10%. In all cases, the uncertainty of the vitiated flow was smaller than that of the clean air results.

CONCLUSIONS

One of the difficulties of a study such as this is to try and draw conclusions that can be applicable to other flows. To this end, a few tentative observations are given.

First, the uncertainty in the individual kinetic terms does not translate to an equivalent level of uncertainty in bulk quantities such as temperature and pressure. It is true that some of the individual reaction rates and species concentrations have significant differences between different kinetic schemes, but that is of little interest to engine designers who are mainly interested in heat release. However, the ignition delay time did have a similar level of uncertainty to that of the individual reactions, with the bounds of uncertainty being a factor of three away from the baseline result. Because of the size of this uncertainty, the ignition process will be one of significant uncertainty when modeled.

Another observation is that the blow-out time exhibited a significantly smaller uncertainty than the ignition delay time. So a combustor that has a residence time close to the blow-off limit will have less uncertainty in predictions of performance compared to the simulation of the ignition process, where the ignition delay time is an important parameter.

The final observation is that vitiation does have an effect on the combustion process, though not a significant one. In all cases, the changes in the results seemed to be similar to the uncertainty caused by the chemical kinetics. Of note was that the results of the vitiated and nonvitiated HDCR simulations exhibited the same trends in thrust results, just offset from each other by a constant value. This indicated a simple thermodynamic scaling would be enough to compensate for the effects of vitiation as the kinetics are not affected in any significant way.

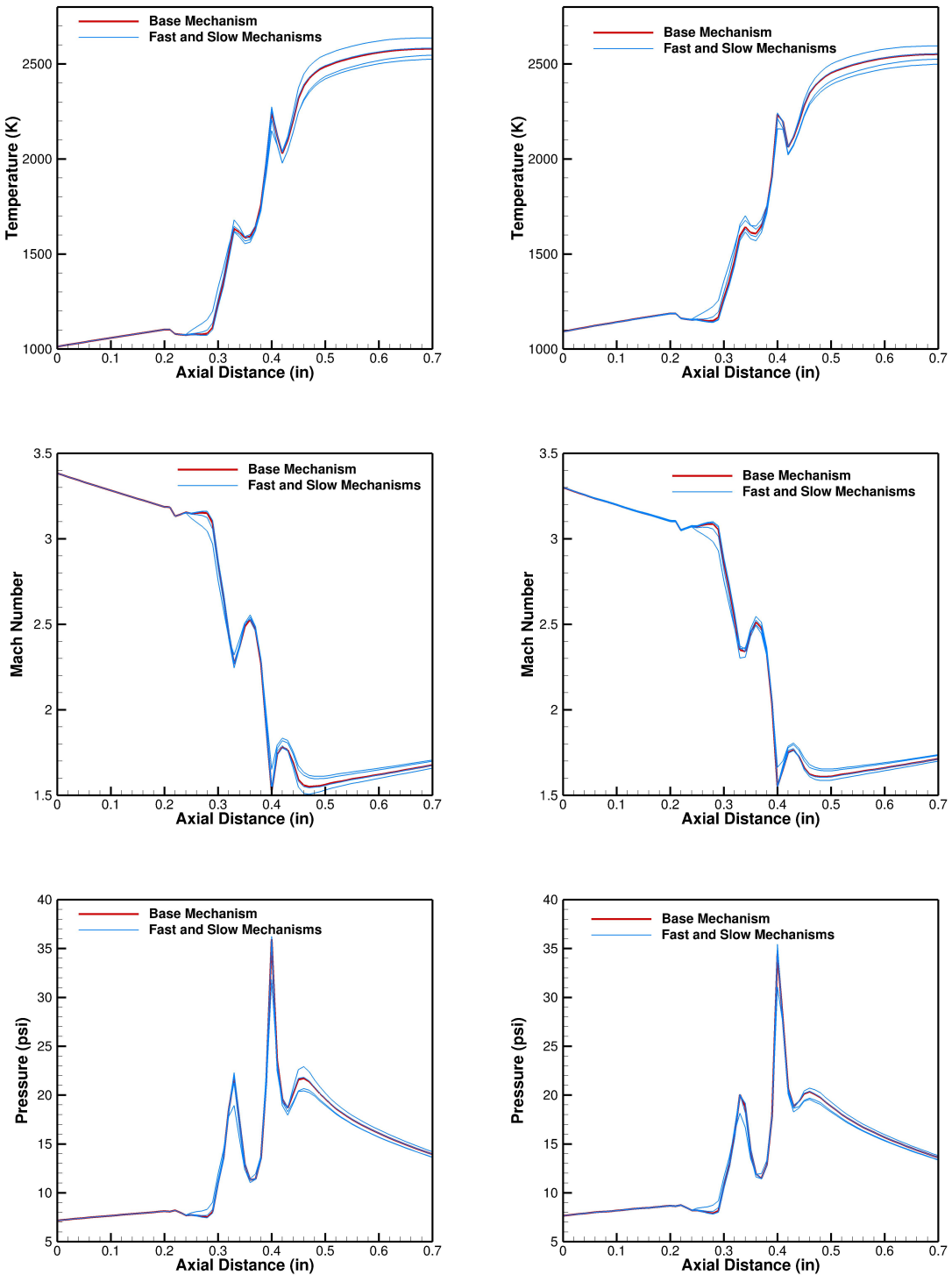

Figure 11. 1D properties of HCD simulations. Clean air results on the left and vitiated air on the right. Red line shows baseline results.

REFERENCES

[1] Mehta, U. B., Eklund, D. R., Romero, V. J., Pearce, J. A., and Keim, N. S., ***Simulation Credibility: Advances in Verification, Validation and Uncertainty Quantification***, Tech. Rep. JANNAF/GL-2016-0001, JANNAF (2016).

[2] Pellett, G. L., Vaden, S. N., and Wilson, L. G., ***Gaseous Surrogate Hydrocarbons for a HiFire Scramjet that Mimic Opposed Jet Extinction Limits for Cracked JP Fuels***, in *JANNAF 55th Propulsion Meeting, 42nd Combustion Meeting, 30th Air-Breathing Propulsion, 30th Exhaust Plume Technology, 24th Propulsion Systems Hazards and 12th Spirits Users Group Joint Subcommittee Meeting, Newton, MA*, page JANNAF (2008).

[3] Cabel, K. F., Hass, N. E., Storch, A. M., and Gruber, M., ***HIFiRE Direct-Connect Rig (HDCR) Phase I Scramjet Test Results from the NASA Langley Arc-Heated Scramjet Test Facility***, in *17th AIAA International Space Planes and Hypersonic Systems and Technologies Conference*, pages AIAA–2011–2248 (2011).

[4] Hass, N., Cabell, K. F., and Storch, A. M., ***HIFiRE Direct-Connect Rig (HDCR) Phase I Ground Test Results from the NASA Langley Arc-Heated Scramjet Test Facility***, in *JANNAF 43rd Combustion, 31st Airbreathing Joint Meeting, La Jolla, California*, pages JANNAF–672 (2009).

[5] K. R. Jackson and M. R. Gruber and S. Buccellato, ***HIFiRE Flight 2: A Program Overview***, JANNAF Journal of Propulsion and Energetics, 6 (2) (2016).

[6] Luo, Z., Yoo, C. S., Richardson, E. S., Chen, J. H., Law, C. K., and Lu, T. F., ***Chemical Explosive Mode Analysis for a Turbulent Lifted Ethylene Jet Flame in Highly-Heated Coflow***, Combustion and Flame, 159 (1):265–274 (2012).

[7] Baulch, D. L., Cobos, C. J., Cox, R. A., Esser, C., Frank, P., Just, T., Kerr, J. A., Pilling, M. J., Troe, J., Walker, R. W., and Warnatz, J., ***Evaluated Kinetic Data for Combustion Modeling***, J. Phys. Chem. Ref. Data, **21**(3):411–734 (1992).

[8] Baulch, D. L., Cobos, C. J., Cox, R. A., Frank, P., Hayman, G., Just, T., Kerr, J. A., Murrels, T., Pilling, M. J., Troe, J., Walker, R. W., and Warnatz, J., ***Evaluated Kinetic Data for Combustion Modeling: Supplement I***, J. Phys. Chem. Ref. Data, **23**(6):847–1033 (1994).

[9] Baulch, D. L., Bowman, C. T., Cobos, C. J., Cox, R. A., Just, T., Kerr, J. A., Pilling, M. J., Stocker, D., Troe, J., Tsang, W., Walker, R. W., and Warnatz, J., ***Evaluated Kinetic Data for Combustion Modeling: Supplement II***, J. Phys. Chem. Ref. Data, **34**(3):757–1397 (2005).

[10] Sklar, A. A., Stone, R., Magaha, B., Philpott, J., Cresci, D., and Osborne, J., ***Test Media Effects on the Performance of a Heavy-Weight, Hydrocarbon Fueled, Direct Connect Rectangular Scramjet Combustor***, in *JANNAF 44th Combustion, 32nd Airbreathing Joint Meeting, Arlington, Virginia*, page JANNAF (2011).

[11] Gaffney, R. L. and Norris, A. T., ***Design of Mach-3 Nozzle for TBCC Testing in the NASA LaRC 8-Ft High Temperature Tunnel***, in *26th AIAA Aerodynamic Measurement Technology and Ground Testing Conference, Seattle, Washington*, pages AIAA–2008–3703 (2008).

[12] Baurle, R. A., ***VULCAN-CFD User Manual***, `https://vulcan-cfd.larc.nasa.gov` (2017).

[13] Pellett, G. L., Bruno, C., and Chinitz, W., ***Review of Air Vitiation Effects on Scramjet Ignition and Flameholding Combustion Processes***, in *38th AIAA/ASME/SAE/ASEE Joint Propulsion Conference and Exhibit, Indianapolis, Indiana*, pages AIAA–2002–3880 (2002).

APPENDIX A

No.	Reaction	A	b	E	UF
1	H+O2 → O+OH	8.30E+13	0.0	14413.0	1.090
2	O+H2 → H+OH	5.00E+04	2.7	6290.0	3.160
3	OH+H2 → H+H2O	2.16E+08	1.5	3430.0	2.000
4	OH+OH → O+H2O	3.57E+04	2.4	-2110.0	2.000
5	H+H+M → H2+M	1.00E+18	-1.0	0.0	3.160
	Third Body Data				
	H2 = 0.0 H2O = 0.0 CH4 = 2. CO2 = 0.0,				
	C2H6 = 3.0 C2H2 = 3.0 C2H4 = 3.0				
6	H+H+H2 → H2+H2	9.00E+16	-0.6	0.0	3.160
7	H+H+H2O → H2+H2O	6.00E+19	-1.2	0.0	3.160
8	H+H+CO2 → H2+CO2	5.50E+20	-2.0	0.0	3.160
9	H+OH+M → H2O+M	2.20E+22	-2.0	0.0	2.000
	Third Body Data				
	H2 = 0.73 H2O = 3.65 CH4 = 2.0 C2H6 = 3.0				
	C2H2 = 3.0 C2H4 = 3.0				
10	O+H+M → OH+M	5.00E+17	-1.0	0.0	5.000
	Third Body Data				
	H2 = 2.0 H2O = 6.0 CH4 = 2.0 CO = 1.5				
	CO2 = 2.0 C2H6 = 3.0 C2H2 = 3.0 C2H4 = 3.0				
11	O+O+M → O2+M	1.20E+17	-1.0	0.0	2.000
	Third Body Data				
	H2 = 2.4 H2O = 15.4 CH4 = 2.0 CO = 1.75				
	CO2 = 3.6 C2H6 = 3.0 C2H2 = 3.0 C2H4 = 3.0				
12	H+O2+M → HO2+M	2.80E+18	-0.9	0.0	1.250
	Third Body Data				
	O2 = 0.0 H2O = 0.0 CO = 0. CO2 = 1.5				
	C2H6 = 1.5 N2 = 0.0 C2H2 = 3.0 C2H4 = 3.0				
13	H+O2+O2 → HO2+O2	3.00E+20	-1.7	0.0	3.160
14	H+O2+H2O → HO2+H2O	1.65E+19	-0.8	0.0	3.160
15	H+O2+N2 → HO2+N2	2.60E+19	-1.2	0.0	3.160
16	OH+OH(+M) → H2O2(+M)	7.40E+13	-0.4	0.0	2.500
	Low pressure limit: 2.30000E+18 -9.00000E-01 -1.70000E+03				
	TROE centering: 7.34600E-01 9.40000E+01 1.75600E+03 5.18200E+03				
	Third Body Data				
	H2 = 2.0 H2O = 6.0 CH4 = 2.0 CO = 1.5				
	CO2 = 2.0 C2H6 = 3.0 C2H2 = 3.0 C2H4 = 3.0				
17	HO2+H → O+H2O	3.97E+12	0.0	671.0	2.000
18	HO2+H → O2+H2	1.66E+13	0.0	820.0	2.000
19	HO2+H → OH+OH	7.08E+13	0.0	300.0	2.000
20	HO2+O → OH+O2	2.00E+13	0.0	0.0	3.160
21	HO2+OH → O2+H2O	4.64E+13	0.0	-500.0	1.580
22	HO2+HO2 → O2+H2O2	1.30E+11	0.0	-1630.0	3.000
	Declared duplicate reaction				
23	HO2+HO2 → O2+H2O2	4.20E+14	0.0	12000.0	3.000
	Declared duplicate reaction				
24	H2O2+H → HO2+H2	1.21E+07	2.0	5200.0	5.000
25	H2O2+H → OH+H2O	1.00E+13	0.0	3600.0	5.000

No.	Reaction	A	b	E	UF
26	H2O2+O → OH+HO2	9.63E+06	2.0	4000.0	3.000
27	H2O2+OH → HO2+H2O	1.75E+12	0.0	320.0	3.000
	Declared duplicate reaction				
28	H2O2+OH → HO2+H2O	5.80E+14	0.0	9560.0	3.000
	Declared duplicate reaction				
29	CO+O+M → CO2+M	6.02E+14	0.0	3000.0	2.500
	Third Body Data				
	H2 = 2.0 O2 = 6.0 H2O = 6.0 CH4 = 2.0				
	CO = 1.5 CO2 = 3.5 C2H6 = 3.0 C2H2 = 3.0 C2H4 = 3.0				
30	CO+OH → CO2+H	4.76E+07	1.2	70.0	3.160
31	CO+H2(+M) → CH2O(+M)	4.30E+07	1.5	79600.0	5.000
	Low pressure limit: 5.07000E+27 -3.42000E+00 8.43500E+04				
	TROE centering: 9.32000E-01 1.97000E+02 1.54000E+03 1.03000E+04				
	Third Body Data				
	H2 = 2.0 H2O = 6.0 CH4 = 2.0 CO = 1.5				
	CO2 = 2.0 C2H6 = 3.0 C2H2 = 3.0 C2H4 = 3.0				
32	CO+O2 → CO2+O	2.50E+12	0.0	47800.0	2.000
33	CO+HO2 → CO2+OH	1.50E+14	0.0	23600.0	2.000
34	CH+O → CO+H	5.70E+13	0.0	0.0	3.160
35	CH+OH → HCO+H	3.00E+13	0.0	0.0	5.000
36	CH+H2 → CH2+H	1.11E+08	1.8	1670.0	1.450
37	CH+H2O → CH2O+H	5.71E+12	0.0	-755.0	5.000
38	CH+O2 → HCO+O	3.30E+13	0.0	0.0	5.000
39	CH+CO(+M) → HCCO(+M)	5.00E+13	0.0	0.0	5.000
	Low pressure limit: 2.69000E+28 -3.74000E+00 1.93600E+03				
	TROE centering: 5.75700E-01 2.37000E+02 1.65200E+03 5.06900E+03				
	Third Body Data				
	H2 = 2.0 H2O = 6.0 CH4 = 2.0 CO = 1.5				
	CO2 = 2.0 C2H6 = 3.0 C2H2 = 3.0 C2H4 = 3.0				
40	CH+CO2 → HCO+CO	3.40E+12	0.0	690.0	5.000
41	HCO+H(+M) → CH2O(+M)	1.09E+12	0.5	-260.0	5.000
	Low pressure limit: 1.35000E+24 -2.57000E+00 1.42500E+03				
	TROE centering: 7.82400E-01 2.71000E+02 2.75500E+03 6.57000E+03				
	Third Body Data				
	H2 = 2.0 H2O = 6.0 CH4 = 2.0 CO = 1.5				
	CO2 = 2.0 C2H6 = 3.0 C2H2 = 3.0 C2H4 = 3.0				
42	HCO+H → CO+H2	7.34E+13	0.0	0.0	2.000
43	HCO+O → CO+OH	3.00E+13	0.0	0.0	2.000
44	HCO+O → CO2+H	3.00E+13	0.0	0.0	2.000
45	HCO+OH → CO+H2O	5.00E+13	0.0	0.0	2.000
46	HCO+M → CO+H+M	1.87E+17	-1.0	17000.0	3.160
	Third Body Data				
	H2 = 2.0 H2O = 6.0 CH4 = 2.0 CO = 1.5				
	CO2 = 2.0 C2H6 = 3.0 C2H2 = 3.0 C2H4 = 3.0				
47	HCO+O2 → CO+HO2	7.60E+12	0.0	400.0	1.580
48	CH2+H(+M) → CH3(+M)	2.50E+16	-0.8	0.0	5.000
	Low pressure limit: 3.20000E+27 -3.14000E+00 1.23000E+03				
	TROE centering: 6.80000E-01 7.80000E+01 1.99500E+03 5.59000E+03				
	Third Body Data				
	H2 = 2.0 H2O = 6.0 CH4 = 2.0 CO = 1.5				
	CO2 = 2.0 C2H6 = 3.0 C2H2 = 3.0 C2H4 = 3.0				

No.	Reaction	A	b	E	UF
49	CH2+H2 → H+CH3	5.00E+05	2.0	7230.0	5.000
50	CH2+O → HCO+H	8.00E+13	0.0	0.0	5.000
51	CH2+O2 → HCO+OH	1.06E+13	0.0	1500.0	5.000
52	CH2+O2 → CO2+H+H	2.64E+12	0.0	1500.0	5.000
53	CH2+OH → CH2O+H	2.00E+13	0.0	0.0	3.000
54	CH2+OH → CH+H2O	1.13E+07	2.0	3000.0	5.000
55	CH2+HO2 → CH2O+OH	2.00E+13	0.0	0.0	5.000
56	CH2+CO(+M) → CH2CO(+M)	8.10E+11	0.5	4510.0	5.000
	Low pressure limit: 2.69000E+33 -5.11000E+00 7.09500E+03				
	TROE centering: 5.90700E-01 2.75000E+02 1.22600E+03 5.18500E+03				
	Third Body Data				
	H2 = 2.0 H2O = 6.0 CH4 = 2.0 CO = 1.5				
	CO2 = 2.0 C2H6 = 3.0 C2H2 = 3.0 C2H4 = 3.0				
57	CH2+CH → C2H2+H	4.00E+13	0.0	0.0	5.000
58	CH2+CH2 → C2H2+H2	3.20E+13	0.0	0.0	1.580
59	CH2*+N2 → CH2+N2	1.50E+13	0.0	600.0	5.000
60	CH2*+H → CH+H2	3.00E+13	0.0	0.0	5.000
61	CH2*+O → CO+H2	1.50E+13	0.0	0.0	5.000
62	CH2*+O → HCO+H	1.50E+13	0.0	0.0	5.000
63	CH2*+OH → CH2O+H	3.00E+13	0.0	0.0	5.000
64	CH2*+H2 → CH3+H	7.00E+13	0.0	0.0	5.000
65	CH2*+O2 → H+OH+CO	2.80E+13	0.0	0.0	5.000
66	CH2*+O2 → CO+H2O	1.20E+13	0.0	0.0	5.000
67	CH2*+H2O → CH2+H2O	3.00E+13	0.0	0.0	5.000
68	CH2*+CO → CH2+CO	9.00E+12	0.0	0.0	5.000
69	CH2*+CO2 → CH2+CO2	7.00E+12	0.0	0.0	5.000
70	CH2*+CO2 → CH2O+CO	1.40E+13	0.0	0.0	5.000
71	CH2O+H(+M) → CH3O(+M)	5.40E+11	0.5	2600.0	5.000
	Low pressure limit: 2.20000E+30 -4.80000E+00 5.56000E+03				
	TROE centering: 7.58000E-01 9.40000E+01 1.55500E+03 4.20000E+03				
	Third Body Data				
	H2 = 2.0 H2O = 6.0 CH4 = 2.0 CO = 1.5				
	CO2 = 2.0 C2H6 = 3.0 C2H2 = 3.0 C2H4 = 3.0				
72	CH2O+H → HCO+H2	2.30E+10	1.1	3275.0	5.000
73	CH2O+O → HCO+OH	3.90E+13	0.0	3540.0	2.000
74	CH2O+OH → HCO+H2O	3.43E+09	1.2	-447.0	2.000
75	CH2O+O2 → HCO+HO2	1.00E+14	0.0	40000.0	2.000
76	CH2O+HO2 → HCO+H2O2	1.00E+12	0.0	8000.0	3.000
77	CH2O+CH → CH2CO+H	9.46E+13	0.0	-515.0	5.000
78	CH3+H(+M) → CH4(+M)	1.27E+16	-0.6	383.0	2.000
	Low pressure limit: 2.47700E+33 -4.76000E+00 2.44000E+03				
	TROE centering: 7.83000E-01 7.40000E+01 2.94100E+03 6.96400E+03				
	Third Body Data				
	H2 = 2.0 H2O = 6.0 CH4 = 2.0 CO = 1.5				
	CO2 = 2.0 C2H6 = 3.0 C2H2 = 3.0 C2H4 = 3.0				
79	CH3+O → CH2O+H	8.43E+13	0.0	0.0	1.580
80	CH3+OH → CH2+H2O	5.60E+07	1.6	5420.0	3.160
81	CH3+OH → CH2*+H2O	2.50E+13	0.0	0.0	1.300
82	CH3+O2 → O+CH3O	3.08E+13	0.0	28800.0	3.160
83	CH3+O2 → OH+CH2O	3.60E+10	0.0	8940.0	3.160
84	CH3+HO2 → CH4+O2	1.00E+12	0.0	0.0	5.000

No.	Reaction	A	b	E	UF
85	CH3+HO2 → CH3O+OH	1.34E+13	0.0	0.0	5.000
86	CH3+H2O2 → CH4+HO2	2.45E+04	2.5	5180.0	5.000
87	CH3+CH → C2H3+H	3.00E+13	0.0	0.0	5.000
88	CH3+HCO → CH4+CO	8.48E+12	0.0	0.0	2.000
89	CH3+HCO(+M) → CH3CHO(+M)	1.80E+13	0.0	0.0	2.000
	Low pressure limit: 2.20000E+48 -9.58800E+00 5.10000E+03				
	TROE centering: 6.17300E-01 1.30760E+01 2.07800E+03 5.09300E+03				
	Third Body Data				
	H2 = 2.0 H2O = 6.0 CH4 = 2.0 CO = 1.5				
	CO2 = 2.0 C2H6 = 3.0 C2H2 = 3.0 C2H4 = 3.0				
90	CH3+CH2O → CH4+HCO	3.32E+03	2.8	5860.0	3.000
91	CH3+CH2 → C2H4+H	4.00E+13	0.0	0.0	2.500
92	CH3+CH2* → C2H4+H	1.20E+13	0.0	-570.0	2.500
93	CH3+CH3(+M) → C2H6(+M)	2.12E+16	-1.0	620.0	2.000
	Low pressure limit: 1.77000E+50 -9.67000E+00 6.22000E+03				
	TROE centering: 5.32500E-01 1.51000E+02 1.03800E+03 4.97000E+03				
	Third Body Data				
	H2 = 2.0 H2O = 6.0 CH4 = 2.0 CO = 1.5				
	CO2 = 2.0 C2H6 = 3.0 C2H2 = 3.0 C2H4 = 3.0				
94	CH3+CH3 → H+C2H5	4.99E+12	0.1	10600.0	5.000
95	CH3+HCCO → C2H4+CO	5.00E+13	0.0	0.0	5.000
96	CH3O+H → CH2O+H2	2.00E+13	0.0	0.0	2.000
97	CH3O+H → CH3+OH	3.20E+13	0.0	0.0	5.000
98	CH3O+H → CH2*+H2O	1.60E+13	0.0	0.0	5.000
99	CH3O+O → CH2O+OH	1.00E+13	0.0	0.0	5.000
100	CH3O+OH → CH2O+H2O	5.00E+12	0.0	0.0	5.000
101	CH3O+O2 → CH2O+HO2	4.28E-13	7.6	-3530.0	5.000
102	CH4+H → CH3+H2	6.60E+08	1.6	10840.0	5.000
103	CH4+O → CH3+OH	1.02E+09	1.5	8600.0	2.000
104	CH4+OH → CH3+H2O	1.00E+08	1.6	3120.0	1.410
105	CH4+CH → C2H4+H	6.00E+13	0.0	0.0	5.000
106	CH4+CH2 → CH3+CH3	2.46E+06	2.0	8270.0	5.000
107	CH4+CH2* → CH3+CH3	1.60E+13	0.0	-570.0	5.000
108	HCCO+H → CH2*+CO	1.00E+14	0.0	0.0	3.160
109	HCCO+O → H+CO+CO	1.00E+14	0.0	0.0	2.000
110	HCCO+O2 → OH+2CO	1.60E+12	0.0	854.0	5.000
111	HCCO+CH → C2H2+CO	5.00E+13	0.0	0.0	5.000
112	HCCO+CH2 → C2H3+CO	3.00E+13	0.0	0.0	5.000
113	HCCO+HCCO → C2H2+CO+CO	1.00E+13	0.0	0.0	5.000
114	C2H2(+M) → H2CC(+M)	8.00E+14	-0.5	50750.0	5.000
	Low pressure limit: 2.45000E+15 -6.40000E-01 4.97000E+04				
	Third Body Data				
	H2 = 2.0 H2O = 6.0 CH4 = 2.0 CO = 1.5				
	CO2 = 2.0 C2H6 = 3.0 C2H2 = 2.5 C2H4 = 2.5				
115	C2H3(+M) → C2H2+H(+M)	3.86E+08	1.6	37048.2	3.160
	Low pressure limit: 2.56500E+27 -3.40000E+00 3.57987E+04				
	TROE centering: 1.98160E+00 5.38370E+03 4.29320E+00 -7.95000E-02				
	Third Body Data				
	H2 = 2.0 H2O = 6.0 CH4 = 2.0 CO = 1.5				
	CO2 = 2.0 C2H6 = 3.0 C2H2 = 3.0 C2H4 = 3.0				
116	C2H2+O → HCCO+H	1.63E+07	2.0	1900.0	3.000

No.	Reaction	A	b	E	UF
117	C2H2+O → CH2+CO	4.08E+06	2.0	1900.0	2.000
118	C2H2+OH → CH2CO+H	2.18E-04	4.5	-1000.0	3.000
119	C2H2+OH → CH3+CO	4.83E-04	4.0	-2000.0	5.000
120	C2H2+HCO → C2H3+CO	1.00E+07	2.0	6000.0	5.000
121	C2H2+CH3+M → aC3H5+M	2.20E+55	-11.8	35730	1.300
122	H2CC+H → C2H2+H	1.00E+14	0.0	0.0	5.000
123	H2CC+O → CH2+CO	1.00E+14	0.0	0.0	2.000
124	H2CC+OH → CH2CO+H	2.00E+13	0.0	0.0	5.000
125	H2CC+O2 → CO2+CH2	1.00E+13	0.0	0.0	5.000
126	CH2CO+H(+M) → CH2CHO(+M)	3.30E+14	-0.1	8500.0	5.000
	Low pressure limit: 3.80000E+41 -7.64000E+00 1.19000E+04				
	TROE centering: 3.37000E-01 1.70700E+03 3.20000E+03 4.13100E+03				
	Third Body Data				
	H2 = 2.0 H2O = 6.0 CH4 = 2.0 CO = 1.5				
	CO2 = 2.0 C2H6 = 3.0 C2H2 = 3.0 C2H4 = 3.0				
127	CH2CO+H → HCCO+H2	5.00E+13	0.0	8000.0	5.000
128	CH2CO+H → CH3+CO	1.50E+09	1.4	2690.0	5.000
129	CH2CO+O → HCCO+OH	1.00E+13	0.0	8000.0	2.000
130	CH2CO+O → CH2+CO2	1.75E+12	0.0	1350.0	2.000
131	CH2CO+OH → HCCO+H2O	7.50E+12	0.0	2000.0	5.000
132	C2H3+H(+M) → C2H4(+M)	6.08E+12	0.3	280.0	5.000
	Low pressure limit: 1.40000E+30 -3.86000E+00 3.32000E+03				
	TROE centering: 7.82000E-01 2.07500E+02 2.66300E+03 6.09500E+03				
	Third Body Data				
	H2 = 2.0 H2O = 6.0 CH4 = 2.0 CO = 1.5				
	CO2 = 2.0 C2H6 = 3.0 C2H2 = 3.0 C2H4 = 3.0				
133	C2H3+H → C2H2+H2	3.00E+13	0.0	0.0	2.500
134	C2H3+H → H2CC+H2	6.00E+13	0.0	0.0	2.500
135	C2H3+O → CH2CO+H	4.80E+13	0.0	0.0	3.000
136	C2H3+O → CH3+CO	4.80E+13	0.0	0.0	5.000
137	C2H3+OH → C2H2+H2O	3.01E+13	0.0	0.0	3.000
138	C2H3+O2 → C2H2+HO2	1.34E+06	1.6	-383.4	5.000
139	C2H3+O2 → CH2CHO+O	3.00E+11	0.3	11.0	5.000
140	C2H3+O2 → HCO+CH2O	4.60E+16	-1.4	1010.0	3.160
141	C2H3+HO2 → CH2CHO+OH	1.00E+13	0.0	0.0	3.000
142	C2H3+H2O2 → C2H4+HO2	1.21E+10	0.0	-596.0	5.000
143	C2H3+HCO → C2H4+CO	9.03E+13	0.0	0.0	3.000
144	C2H3+CH3 → C2H2+CH4	3.92E+11	0.0	0.0	3.000
145	C2H3+CH3(+M) → C3H6(+M)	2.50E+13	0.0	0.0	1.500
	Low pressure limit: 4.27000E+58 -1.19400E+01 9.76980E+03				
	TROE centering: 1.75000E-01 1.34060E+03 6.00000E+04 1.01398E+04				
	Third Body Data				
	H2 = 2.0 H2O = 6.0 CH4 = 2.0 CO = 1.5				
	CO2 = 2.0 C2H6 = 3.0 C2H2 = 3.0 C2H4 = 3.0				
146	C2H3+CH3 → aC3H5+H	1.50E+24	-2.8	18618.0	5.000
147	CH2CHO → CH3+CO	7.80E+41	-9.1	46900.0	2.000
148	CH2CHO+H(+M) → CH3CHO(+M)	1.00E+14	0.0	0.0	5.000
	Low pressure limit: 5.20000E+39 -7.29700E+00 4.70000E+03				
	TROE centering: 5.50000E-01 8.90000E+03 4.35000E+03 7.24400E+03				
	Third Body Data				
	H2 = 2.0 H2O = 6.0 CH4 = 2.0 CO = 1.5				
	CO2 = 2.0 C2H6 = 3.0 C2H2 = 3.0 C2H4 = 3.0				

No.	Reaction	A	b	E	UF
149	CH2CHO+H → CH3+HCO	9.00E+13	0.0	0.0	5.000
150	CH2CHO+H → CH2CO+H2	2.00E+13	0.0	4000.0	5.000
151	CH2CHO+O → CH2CO+OH	2.00E+13	0.0	4000.0	5.000
152	CH2CHO+OH → CH2CO+H2O	1.00E+13	0.0	2000.0	3.000
153	CH2CHO+O2 → CH2CO+HO2	1.40E+11	0.0	0.0	5.000
154	CH2CHO+O2 → CH2O+CO+OH	1.80E+10	0.0	0.0	2.000
155	C2H4(+M) → H2+H2CC(+M)	8.00E+12	0.4	88770.0	5.000
	Low pressure limit: 7.00000E+50 -9.31000E+00 9.98600E+04				
	TROE centering: 7.34500E-01 1.80000E+02 1.03500E+03 5.41700E+03				
	Third Body Data				
	H2 = 2.0 H2O = 6.0 CH4 = 2.0 CO = 1.5				
	CO2 = 2.0 C2H6 = 3.0 C2H2 = 3.0 C2H4 = 3.0				
156	C2H4+H(+M) → C2H5(+M)	1.08E+12	0.5	1820.0	3.000
	Low pressure limit: 1.20000E+42 -7.62000E+00 6.97000E+03				
	TROE centering: 9.75300E-01 2.10000E+02 9.84000E+02 4.37400E+03				
	Third Body Data				
	H2 = 2.0 H2O = 6.0 CH4 = 2.0 CO = 1.5				
	CO2 = 2.0 C2H6 = 3.0 C2H2 = 3.0 C2H4 = 3.0				
157	C2H4+H → C2H3+H2	5.07E+07	1.9	12950.0	3.000
158	C2H4+O → OH+C2H3	1.51E+07	1.9	3740.0	5.000
159	C2H4+O → CH3+HCO	1.92E+07	1.8	220.0	2.000
160	C2H4+O → CH2+CH2O	3.84E+05	1.8	220.0	5.000
161	C2H4+OH → C2H3+H2O	3.60E+06	2.0	2500.0	4.000
162	C2H4+O2 → C2H3+HO2	4.22E+13	0.0	60800.0	5.000
163	C2H4+HO2 → CH3CHO+OH	2.00E+12	0.0	14000.0	5.000
164	C2H4+HCO → C2H5+CO	1.00E+07	2.0	8000.0	5.000
165	C2H4+CH2 → aC3H5+H	2.00E+13	0.0	6000.0	5.000
166	C2H4+CH2* → H2CC+CH4	5.00E+13	0.0	0.0	5.000
167	C2H4+CH2* → aC3H5+H	5.00E+13	0.0	0.0	5.000
168	C2H4+CH3 → C2H3+CH4	2.27E+05	2.0	9200.0	2.000
169	C2H4+CH3 → nC3H7	3.30E+11	0.0	7700.0	1.300
170	C2H5+H(+M) → C2H6(+M)	5.21E+17	-1.0	1580.0	5.000
	Low pressure limit: 1.99000E+41 -7.08000E+00 6.68500E+03				
	TROE centering: 8.42200E-01 1.25000E+02 2.21900E+03 6.88200E+03				
	Third Body Data				
	H2 = 2.0 H2O = 6.0 CH4 = 2.0 CO = 1.5				
	CO2 = 2.0 C2H6 = 3.0 C2H2 = 3.0 C2H4 = 3.0				
171	C2H5+H → C2H4+H2	2.00E+12	0.0	0.0	3.000
172	C2H5+O → CH3+CH2O	1.60E+13	0.0	0.0	5.000
173	C2H5+O → CH3CHO+H	8.02E+13	0.0	0.0	2.000
174	C2H5+O2 → C2H4+HO2	2.00E+10	0.0	0.0	2.000
175	C2H5+HO2 → C2H6+O2	3.00E+11	0.0	0.0	2.000
176	C2H5+HO2 → C2H4+H2O2	3.00E+11	0.0	0.0	2.000
177	C2H5+HO2 → CH3+CH2O+OH	2.40E+13	0.0	0.0	5.000
178	C2H5+H2O2 → C2H6+HO2	8.70E+09	0.0	974.0	5.000
179	C2H5+HCO → C2H6+CO	1.20E+14	0.0	0.0	3.000
180	C2H6+H → C2H5+H2	1.15E+08	1.9	7530.0	2.000
181	C2H6+O → C2H5+OH	8.98E+07	1.9	5690.0	2.000
182	C2H6+OH → C2H5+H2O	3.54E+06	2.1	870.0	2.000
183	C2H6+CH2* → C2H5+CH3	4.00E+13	0.0	-550.0	5.000

No.	Reaction	A	b	E	UF
184	C2H6+CH3 → C2H5+CH4	6.14E+06	1.7	10450.0	2.000
185	aC3H5+H(+M) → C3H6(+M)	2.00E+14	0.0	0.0	5.000
	Low pressure limit: 1.33000E+60 -1.20000E+01 5.96780E+03				
	TROE centering: 2.00000E-02 1.09660E+03 1.09660E+03 6.85950E+03				
	Third Body Data				
	H2 = 2.0, H2O = 6.0, CH4 = 2.0, CO = 1.5, CO2 = 2.0,				
	C2H6 = 3.0, C2H2 = 3.0, C2H4 = 3.0				
186	aC3H5+H → H2CC+CH4	2.00E+13	0.0	2000.0	5.000
187	aC3H5+HO2 → C3H6+O2	2.66E+12	0.0	0.0	5.000
188	aC3H5+HO2 → OH+C2H3+CH2O	6.60E+12	0.0	0.0	5.000
189	aC3H5+HCO → C3H6+CO	6.00E+13	0.0	0.0	5.000
190	C3H6+H(+M) → nC3H7(+M)	1.33E+13	0.0	3260.7	1.500
	Low pressure limit: 6.26000E+38 -6.66000E+00 7.00000E+03				
	TROE centering: 1.00000E+00 1.00000E+03 1.31000E+03 4.80970E+04				
	Third Body Data				
	H2 = 2.0, H2O = 6.0, CH4 = 2.0, CO = 1.5, CO2 = 2.0, C2H6 = 3.0				
191	C3H6+H → C2H4+CH3	1.60E+22	-2.4	11180.0	5.000
192	C3H6+H → aC3H5+H2	1.70E+05	2.5	2490.0	2.000
193	C3H6+O → CH2CO+CH3+H	1.20E+08	1.6	327.0	5.000
194	C3H6+O → C2H5+HCO	3.50E+07	1.6	-972.0	5.000
195	C3H6+O → aC3H5+OH	1.80E+11	0.7	5880.0	3.000
196	C3H6+OH → aC3H5+H2O	3.10E+06	2.0	-298.0	2.000
197	C3H6+HO2 → aC3H5+H2O2	9.60E+03	2.6	13910.0	5.000
198	C3H6+CH3 → aC3H5+CH4	2.20E+00	3.5	5675.0	1.400
199	nC3H7+H → C2H5+CH3	3.70E+24	-2.9	12505.0	5.000
200	nC3H7+H → C3H6+H2	1.80E+12	0.0	0.0	2.000
201	nC3H7+O → C2H5+CH2O	9.60E+13	0.0	0.0	2.000
202	nC3H7+OH → C3H6+H2O	2.40E+13	0.0	0.0	3.000
203	nC3H7+O2 → C3H6+HO2	9.00E+10	0.0	0.0	3.000
204	nC3H7+HO2 → C2H5+OH+CH2O	2.40E+13	0.0	0.0	5.000
205	nC3H7+CH3 → CH4+C3H6	1.10E+13	0.0	0.0	1.700
206	C2H3+C2H5 → aC3H5+CH3	3.90E+32	-5.2	19747.0	3.000